Mechanistic model for booster doses effectiveness in healthy, cancer, and immunosuppressed patients infected with SARS-CoV-2

Chrysovalantis Voutouri[a,b], C. Corey Hardin[c], Vivek Naranbhai[d,e,f] 🆔, Mohammad R. Nikmaneshi[a,g], Melin J. Khandekar[h], Justin F. Gainor[d], Triantafyllos Stylianopoulos[b,1], Lance L. Munn[a,1], and Rakesh K. Jain[a,1] 🆔

SARS-CoV-2 vaccines are effective at limiting disease severity, but effectiveness is lower among patients with cancer or immunosuppression. Effectiveness wanes with time and varies by vaccine type. Moreover, previously prescribed vaccines were based on the ancestral SARS-CoV-2 spike-protein that emerging variants may evade. Here, we describe a mechanistic mathematical model for vaccination-induced immunity. We validate it with available clinical data and use it to simulate the effectiveness of vaccines against viral variants with lower antigenicity, increased virulence, or enhanced cell binding for various vaccine platforms. The analysis includes the omicron variant as well as hypothetical future variants with even greater immune evasion of vaccine-induced antibodies and addresses the potential benefits of the new bivalent vaccines. We further account for concurrent cancer or underlying immunosuppression. The model confirms enhanced immunogenicity following booster vaccination in immunosuppressed patients but predicts ongoing booster requirements for these individuals to maintain protection. We further studied the impact of variants on immunosuppressed individuals as a function of the interval between multiple booster doses. Our model suggests possible strategies for future vaccinations and suggests tailored strategies for high-risk groups.

SARS-CoV-2 | mRNA1273 | BNT162b2 | Ad26.COV2.S | booster dose

COVID-19 has created unprecedented challenges for healthcare systems and society. Despite the effectiveness and widespread availability of vaccines in many countries, the pandemic persists. The large unvaccinated population, incomplete vaccine response in immunosuppressed patients, and waning immunity following vaccination all contribute to the persistence of the crisis. The unvaccinated and immunosuppressed populations, moreover, can allow for continued viral spread and emergence of new SARS-CoV-2 variants (1, 2). Understanding the limits of vaccine-induced immunity is vital to ongoing efforts to address the COVID-19 pandemic. Indeed, numerous clinical studies are taking place worldwide to evaluate the protective capacity of mRNA and vector vaccines over time against the ancestral and emerging variants of the SARS-CoV-2 virus, for those vaccinated with or without prior infection as well as for patients who may have a suboptimal vaccine response due to underlying disease (e.g., cancer) or due to treatment with immunosuppressive therapies (e.g., chemotherapy) (3–14). Based on these studies, it is now accepted that booster doses are required to maintain sufficient levels of immunity, particularly in patients with cancer who receive chemotherapy or other immunosuppressive treatment or for other individuals receiving immunomodulatory medications (4, 7, 9, 13–18). These findings have been rapidly incorporated into public health recommendations, but it remains uncertain how long booster doses ensure immunity, how effective they are against emerging variants or how to tailor vaccine regimens in high-risk populations. There is currently no proven framework for prospective prediction of optimal vaccine schedules in a dynamically evolving pandemic, especially for the high-risk patient populations most likely to suffer from deleterious consequences of waning immunity.

Computational modeling can be used to explore the biological mechanisms of COVID-19 to identify better treatment strategies (19–27). We recently developed a mechanistic model of COVID-19 that includes lung infection by the SARS-CoV-2 virus, the innate and adaptive immune responses, local and systemic thrombosis and a pharmacokinetic/pharmacodynamic (PK/PD) model of the dissemination of virus, cytokines, and microthrombi throughout the body (28). This mechanistic model consists of a series of differential equations which describe the dynamics of the above processes and enable the testing of hypotheses about the interactions between viral infection and various components of the immune response to that infection. Here, we address the need for predictions of vaccine effectiveness over time by building on our mathematical framework to account for

Significance

Current SARS-CoV-2 vaccines are effective at preventing COVID-19 or limiting disease severity in healthy individuals, but effectiveness is lower among patients with cancer or immunosuppression. Here, we address the need for predictions of vaccine effectiveness over time by building on our mathematical framework to account for vaccination-induced immunity. A booster dose of both mRNA vaccines can induce a robust enhancement of both antibody levels and numbers of pertinent types of adaptive immune cells, which is predicted to provide sufficient protection for more than 1 y in healthy patients. However, our model suggests that for immunosuppressed people or patients with cancer receiving an immunosuppressive treatment, the booster effect may wane and should be given boosters on a more frequent basis.

vaccination-induced immunity. We include the separate mechanisms of mRNA and viral-vector vaccines in healthy, immunosuppressed, and patients with cancer. The model accounts for translation of viral antigens, the production of antigen and its presentation by dendritic cells, the subsequent activation of T cells and B cells to create CD4$^+$ and CD8$^+$ effector and memory T cells, as well as short-lived and long-lived plasma (antibody-secreting) B cells. We also consider various anti-cancer therapies, including chemotherapy and PD-L1/PD-1-immune checkpoint blockade (Fig. 1).

With this modeling approach, we seek to develop hypotheses about possible consequences for the immune response to viral infection with impairments in specific arms of the immune system. Such hypotheses should, of course, be subject to verification by experimental data. The large number of parameters in our model would be difficult to precisely validate against clinical data. As such, it is distinct from data-driven "statistical" models (29, 30, 31) which seek to develop predictors of individual patients' courses though the analysis of large clinical datasets. Instead, we seek to develop hypotheses about possible consequences for the immune response to viral infection with impairments in specific arms of the immune system.

We first parameterize our model with clinical data for vaccinated healthy individuals and patients with cancer, and then we compare model predictions of temporal changes in antibody levels directed against the SARS-CoV-2 spike protein to clinical data. Subsequently, we use the model to explore the effect of booster vaccine doses among healthy individuals and those with cancer and/or receiving immunosuppressive therapies. We further use the model to explore how specific characteristics of potential new, yet unobserved, viral variants could influence vaccine efficacy. We find that for healthy individuals vaccinated and boosted with mRNA-1273 or BNT-162b2a, robust immunogenicity against the ancestral and delta variant extends beyond a year, in agreement with predictions of pertinent studies (32). Immunogenicity is also significantly enhanced following booster vaccination in patients with cancer on

various anti-cancer therapies and for patients without cancer on immunosuppressive agents, such as B cell depleting therapy, long-term corticosteroids or TNF blockers. However, our model predicts that one or more additional booster doses will be required for these individuals to maintain long-term immunity. Similar results were seen with Ad26.COV2.S, although antibody levels were less than for the mRNA vaccines. Finally, we extend our analysis to the omicron variants, which have been dominant during the recent stage of the pandemic, and then assess the potential benefits of the new bivalent vaccines, which have increased specificity against omicron. We conclude that booster doses with the new vaccines will benefit the at-risk population more than the healthy individuals.

Results

Validation of Model Predictions for SARS-CoV-2 Spike Protein with Available Clinical Data for Healthy Individuals and Cancer Patients. A description of the model is provided in the caption of Fig. 1. The values of the model parameters related to viral infection and the PK/PD of COVID-19 were defined and validated in previous work (28) (and are presented in *SI Appendix*, Table S3). Here, we incorporated additional equations and model parameters related to vaccination-induced immunity, summarized in *SI Appendix*, Table S1. These parameters include the affinity for and uptake rate of vaccine particles by cells, the rate of DNA transcription to mRNA, the production rate of viral antigens, and the degradation rates of the vaccine and the viral antigen. To calculate the baseline values of these parameters, we fitted model predictions to clinical data of average values of anti-spike antibody levels directed against the SARS-CoV-2 spike protein in healthy individuals who received either two doses of the mRNA vaccines (BNT-162b2a or mRNA-1273) or a single dose of the Ad26.COV2.S vaccine presented in our previous work [Fig. 2, Naranbhai V et al. (12)]. Note that these initial fits were not intended to yield parameters that precisely predict the response of
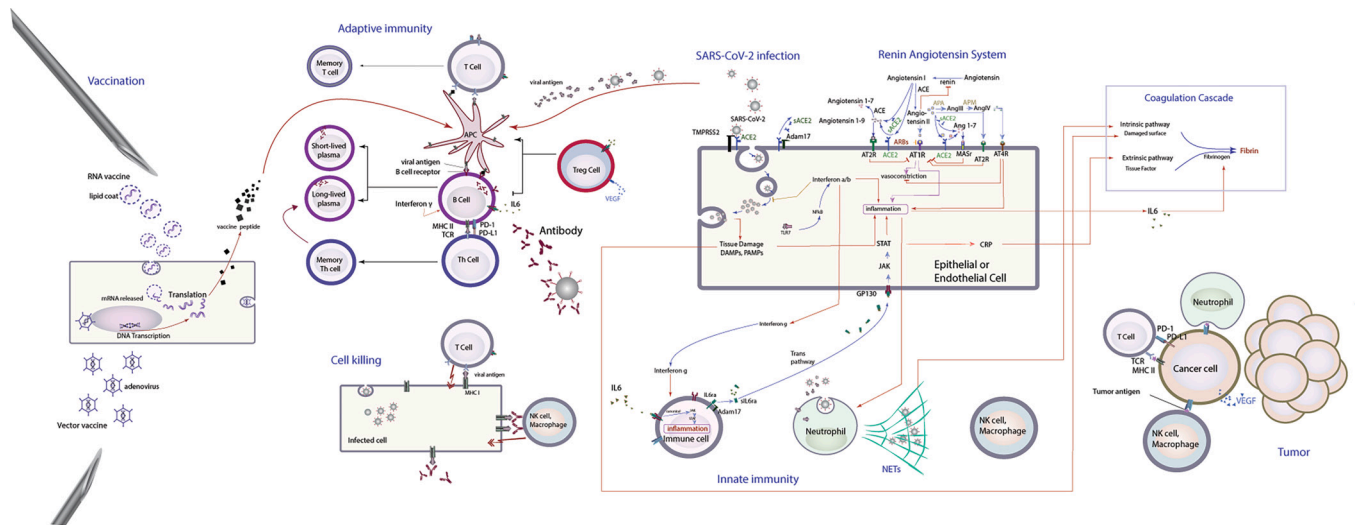

Fig. 1. Schematic representation of the mathematical model. The basic components of the model are: i) a detailed model of lung infection by SARS-CoV-2 that includes innate and adaptive immune responses, known mechanisms of the renin-angiotensin system (RAS) and the coagulation cascade. Intracellular virus initiates inflammatory pathways through toll-like receptors and NFκB, which produces interferons and other inflammatory cytokines. The viral antigens, along with inflammatory cytokines, facilitate activation of naïve B and T cells, creating virus-specific effector cells. Activation of naïve immune cells is controlled by viral antigen strength and the status of immune checkpoint inhibition (specifically PD-L1/PD-1). ii) A PK/PD model of dissemination of viral particles, cytokines, microthrombi, and antibodies in the major organs (lung, heart, liver, brain, spleen, gastro-intestinal, upper body, lower body, torso, cardiac vessels, and the tumor; see *SI Appendix*, Fig. S1). iii) All steps of vaccination-induced immunity for mRNA and vector vaccines, including the translation of viral antigens, the production of antigen-presenting cells by dendritic cells, the subsequent activation of T cells and B cells to create CD4$^+$ and CD8$^+$ effector and memory T cells, as well as short-lived and long-lived plasma (antibody-secreting) B cells. iv) Tumor cells and interactions with the immune system. Proliferation of tumor cells depends on oxygen levels in the tissue, and their death rate on the interaction of cancer cells with immune cells (effector CD8$^+$ T cells, natural killer cells, type 1 macrophages and neutrophils) as well as on the effect of cancer therapy. We assume no tumor cell–virus interactions.

any individual patient but merely to establish baseline values for our further analysis. To quantify the quality of the fit, we provide in the figure caption the χ^2 values, calculated for the model predictions vs. the clinical data. These values are: $\chi^2 = 0.0081$ for the BNT-162b2 vaccine, $\chi^2 = 0.0484$ for the mRNA-1273 vaccine, and $\chi^2 = 0.1139$ for the Ad26.COV2.S vaccine. To account for inherent clinical heterogeneity (which may not be accounted for by any single set of parameter choices) and assess the robustness of our predictions to variations from the best-fit parameter values, we repeated simulations using a range of values within an order of magnitude around the baseline values (*SI Appendix,* Table S1). Simulations were repeated for all possible combinations among parameters taking 100 different values for each parameter. The results are presented in the figures as SE bars from the baseline values.

Subsequently, we compared model predictions with additional data from seven independent clinical studies on booster doses (i.e., a third dose for BNT-162b2a and mRNA-1273 and a second dose for Ad26.COV2.S) for healthy individuals as well as with clinical data of patients living with cancer who had received chemotherapy or PD-L1/PD-1 immune checkpoint blockers and had been vaccinated (8–12, 33, 34). Modifications made to specific model parameters in order to fit various cancer treatments are shown in *SI Appendix,* Table S1. The model was able to provide accurate predictions of antibody levels for all sets of clinical data considered (Fig. 2, and the corresponding χ^2 values in the figure caption) as well as accurate predictions of memory CD4, CD8 cells (35) (*SI Appendix,* Fig. S1).

Antibody levels are directly linked to immune protection from SARS-CoV-2 infection (32); we therefore take predicted antibody levels as a measure of vaccine efficacy. Mathematical modeling of the relationship between antibody concentration and neutralizing titres (20), also justify the use of antibody concentrations as a correlate of protection.

Robustness of Spike-Specific Antibody Levels in Healthy Individuals, Patients with Cancer, and Immunosuppressed Individuals. We assessed the long-term robustness of spike-specific antibody levels by simulating the effects of vaccination over a
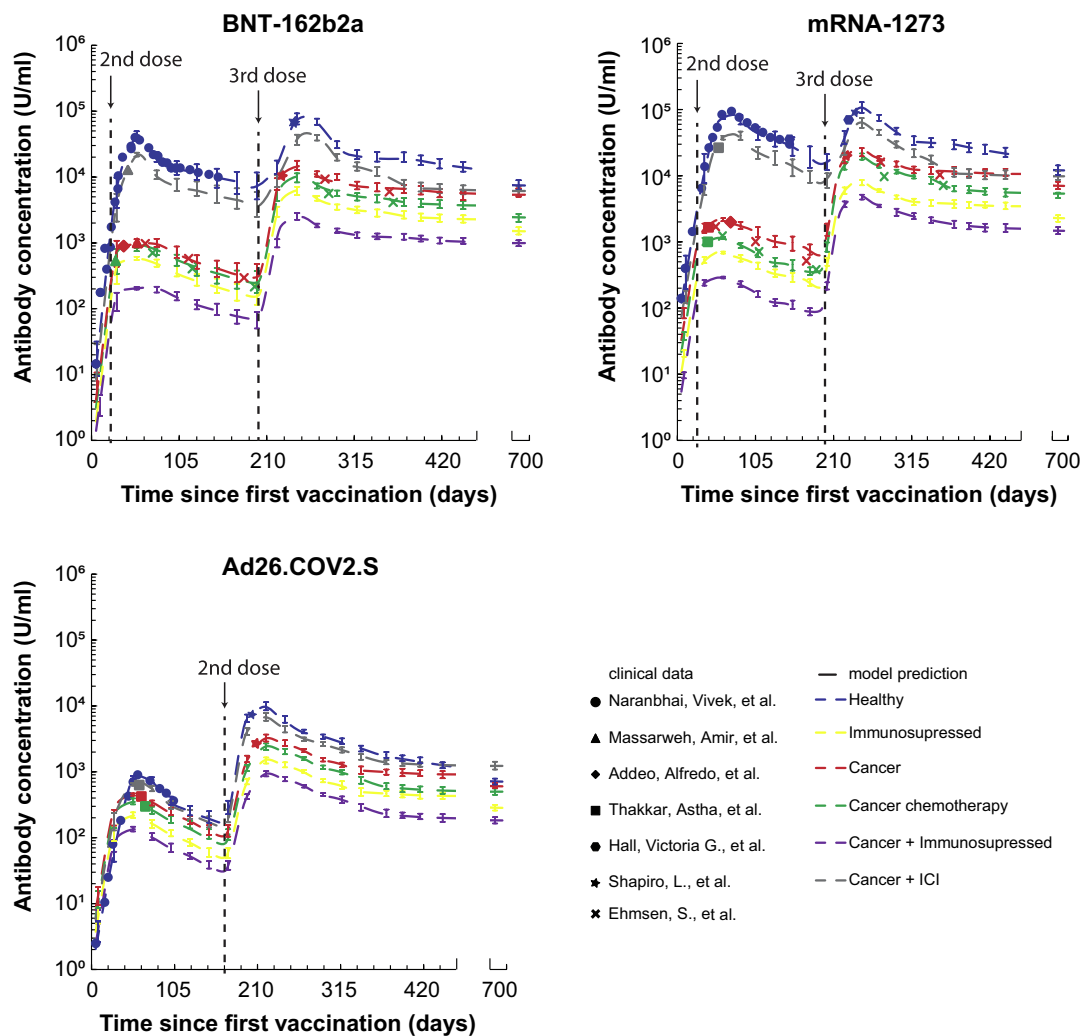

Fig. 2. Model predictions and validation with clinical data of anti-spike antibody levels from vaccinated healthy people and lung cancer patients as a training set. The scatter symbols correspond to clinical data (8–12, 33, 34) and the dash lines to model predictions. The sum of the squared error (i.e., χ^2 value) between the clinical data for each of the 6 studies and the corresponding model predictions for the baseline values of model parameters were calculated. For the temporal variation of antibody levels in healthy: $\chi^2 = 0.0081$ for the BNT-162b2 vaccine, $\chi^2 = 0.0484$ for the mRNA-1273 vaccine, and $\chi^2 = 0.1139$ for the Ad26.COV2.S vaccine. For the single time point data of patients with cancer: Cancer: $\chi^2 = 0.00013$ (BNT-162b2), $\chi^2 = 0.0045$ (mRNA-1273), $\chi^2 = 0.0083$ (Ad26.COV2.S). Cancer+ICI: $\chi^2 = 0.00032$ (BNT-162b2), $\chi^2 = 0.00214$ (mRNA-1273), $\chi^2 = 0.00074$ (Ad26.COV2.S). Cancer + chemotherapy: $\chi^2 = 0.00061$ (BNT-162b2), $\chi^2 = 0.0053$ (mRNA-1273), $\chi^2 = 0.0072$ (Ad26.COV2.S). Error bars present the SE of antibody concentration for all values of model parameters considered. χ^2 is the sum of the squared difference between the clinically measured, Ct_{clin}, and the predicted by the model, Ct_{model}, antibody concentration divided by the number of clinical data n, $\chi^2 = \frac{1}{n}\sum_{i=1}^{n}[(Ct_{clin}-Ct_{clin})_i^2]$.

period of 100 wk (i.e., 700 d), including a third dose for the mRNA vaccines and a second dose of the vector vaccine. Fig. 2 presents the model predictions of anti-spike antibody levels as a function of time. In agreement with clinical studies, the model predicts a significant reduction in the antibody levels in all types of vaccines within 6 mo and a rapid and robust increase in antibody levels following a booster dose. Interestingly, for healthy individuals, the antibody levels following a booster dose are predicted to stay above 10,000 U/ml for the mRNA vaccines and 1,000 U/ml for the vector vaccine for the entire simulated period (i.e., 78 to 80 wk from booster dose) but reach lower values for patients with cancer and particularly for immunosuppressed patients with or without cancer. Antibody levels above 1,000 U/mL (14) have been suggested to correlate with protective immunity. The only exception are patients with cancer that receive PD-L1/PD-1 inhibition; they exhibit the same antibody levels as healthy individuals per our model predictions. Interestingly, our model predicts that healthy individuals receiving a third mRNA vaccination can sustain antibody levels above 1,000 U/mL for a period of 180 wk (*SI Appendix*, Fig. S1). Even though such long-term data from a booster dose are still not available, model predictions agree with the limited data of antibody levels and T cell immune responses available as of now (36–40) (Fig. 2) as well as with predictions made by extrapolating clinical data after a third mRNA vaccination for patients with cancer on chemotherapy, anti-CD20 therapy or on BTK inhibitors (34).

Cell-Mediated Immunity Following Vaccination. We next examined the effects of vaccination on the levels of immune cells that influence the severity of viral infection (Fig. 3 for BNT-

162b2a, *SI Appendix,* Figs. S2 and S3 for mRNA-1273 and AD26.COV2.S, respectively). Within a period of 6 mo from the second dose of the mRNA vaccines, B cell, $CD4^+$, $CD8^+$ T cell and antigen-presenting cell (APC) levels are predicted to drop up to 50%. The decreases in immune cell populations were much less pronounced than the decreases in antibody levels, consistent with recent clinical data (35). For the vector vaccine, the decrease in the 6-mo period is less profound, but the peak levels achieved are also significantly lower compared to the mRNA vaccines. Following a booster dose, there is an enhancement of all immune cell levels against the virus. Healthy individuals and patients with cancer receiving PD-L1/PD-1 inhibition therapy benefitted the most, and at the end of the 100-wk simulation, the levels of all immune cells were up to twice as high as before the booster dose. In contrast, immunosuppressed individuals with or without cancer benefit the least, with a less than 50% increase in APCs and memory B cells, $CD4^+$, and $CD8^+$ T cells.

Vaccine-Induced Protection against Severe Disease Caused by Viral Variants. Next, we investigated the effects of new variants of the virus in patients on immunosuppression who had received a booster dose. Given that initial model validation was performed when the delta variant was dominant, we consider baseline values of virus infection (*SI Appendix*, Table S2) to be related to the delta variant, which was treated as the control. Our data on infection after vaccination are consistent with the reduced efficacy of a 2-dose regimen for Omicron subvariants BA.1, BA.2, BA.4/5, BA.2 L452Q, and BA.2 S704L. However, addition of a booster dose enhances the antibody response against these variants to similar levels seen with the 2-dose regimen with a delta infection. We
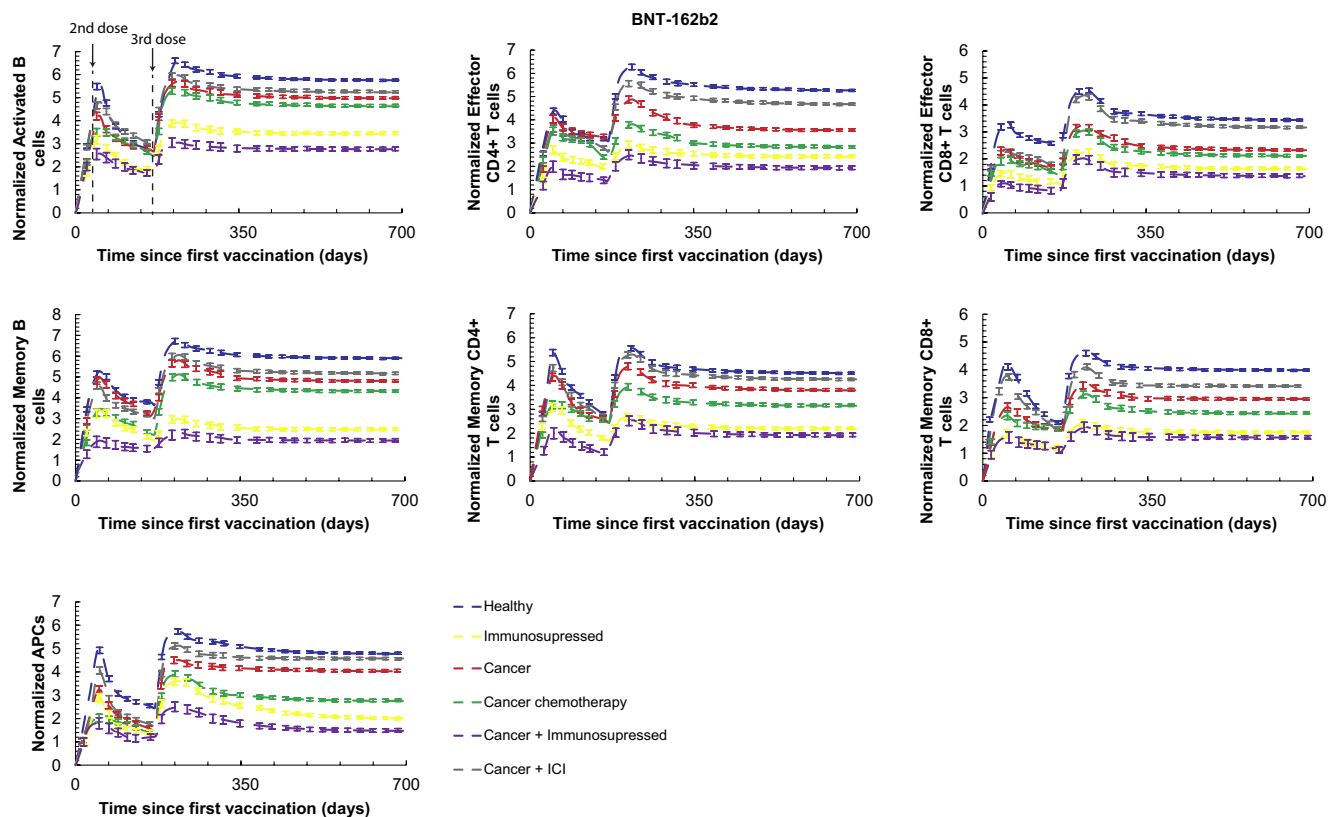
Fig. 3. Vaccination-induced immunity following the BNT-162b2a vaccine in different patient groups. Levels of B cell, $CD4^+$, $CD8^+$ T cell and APCs are depicted for a period of 100 wk following initial vaccination and a booster dose 6 mo later. Values are normalized to the initial value of the corresponding naïve cell type. Error bars present the SE for all values of model parameters considered accounting for interpatient heterogeneity. The initial values of each naïve cell type are: immature dendritic cells 10^3 [cells], Naïve $CD4^+$ T cells 10^3 [cells], Naïve $CD8^+$ T cells 10^3 [cells], Naïve B cells 10^3 [cells].

modulated several parameters in the model to mimic variants that might differ in viral fitness and immune evasion. These include: the affinity of virus for ACE2 (i.e., binding to and detachment from ACE2), the rate of virus internalization into host cells, the replication rate of the internalized virus, the release rate of the virus from infected cells, the clearance rate of viral particles by antibodies, and the activation of immune cells by virus (antigenicity). In our analysis, we accounted separately for variations in each of these parameters either by changing the pertinent rates by 10-fold (mild mutation) or by 100-fold (severe mutation). Exposure to virus was considered to take place 6 mo after the booster dose.

To examine the clinical course following a booster dose and then infection with a variant virus, we compared the predicted values for viral load, coagulation/microthrombi formation in the lungs, oxygen saturation levels and the concentration of memory CD4+, CD8+, and B cells following a booster dose. Results for the BNT-162b2a vaccine are shown in Fig. 4. *SI Appendix*, Figs. S4 and S5 present the corresponding results for the mRNA-1273 and Ad26. COV.S vaccines. We find that variants capable of escaping vaccine-induced immunity can lead to more severe infections characterized by increased viral load, more microthrombi formation and lower arterial oxygen saturation. This becomes more evident for severe mutations and for patients who received a vector vaccine (Fig. 4*B* and *SI Appendix*, Figs. S4 and S5). Furthermore, model predictions indicate a decrease in CD4+ and CD8+ T cells following infection by a variant in agreement with recent clinical data for the Omicron variant (41). The variants that produced the worst clinical metrics were those with reduced immunogenicity, increased ACE2 binding, and decreased antibody-virus binding. Parameters associated with virus replication, internalization, and exocytosis had relatively less effect on clinical trajectories. These data are consistent with recent reports that even after a booster dose, infection with omicron subvariants BA.4 and BA.5 result in lower levels of neutralizing antibodies compared to earlier variants (42).

We further extended our analysis to explore patient heterogeneity, including, in addition to healthy patients, older and immunosuppressed individuals. We repeated simulations for variants with increased ACE2 binding and increased replication rate (Figs. 5 and 6 and *SI Appendix*, Figs. S6–S9). The decrease in memory T cells and in B cells following viral infection is found in all patient types but it is more prominent in immunosuppressed and older individuals compared to young healthy people. This is particularly evident for severe mutations affecting ACE2-binding affinity where the levels of memory T cells and B cells drop by more than 50% compared to the corresponding values of the healthy individuals. The decrease in the memory cell population following infection by a variant is attributed to the fact that the variant can more effectively infect endothelial and epithelial cells, causing an increase in IFNγ, which in turn decreases the concentration of T cells and B cells compared to the ancestral virus. Our results demonstrate that changes in viral parameters of fitness and immune escape may result in more severe infections not only on immunosuppressed patients but even for healthy individuals or older individuals not on immunosuppressive therapies.

Effect of Intervals between Booster Doses on Viral Infection and Immunity. We next simulated different time intervals between a first and a second booster dose for both mRNA and vector vaccines on viral infection and cell immunity. We first repeated the simulations of viral infection by a variant (with severe mutation) for patients on immunosuppression, varying the time interval of the first booster dose from 3 to 6 mo. As before, exposure to virus was considered to take place 6 mo after the booster dose. Model predictions are depicted in Fig. 7 for the BNT-162b2a

vaccine and in *SI Appendix*, Figs. S10 and S11, for the mRNA-1273 and AD26.COV2.S vaccines, respectively. Interestingly, the model predicts a more than 60% reduction in viral load and microthrombi formation (for the mRNA vaccines) and higher levels of memory CD4+ and CD8+ T cells when the first booster is administered after a 6-mo interval compared to a 3-mo interval. In the mathematical model, the activation of CD4+/CD8+ T cells and B cells depends largely on the [PD1-PDL1] complex. Specifically, when [PD1-PDL1] are lower, more CD4+/CD8+ T cells and B cells get activated, resulting in higher concentrations of the corresponding memory cells. The temporal dynamics of [PD1-PDL1] complex formation are affected by booster timing. Results from varying the time delay before the first booster from 3 to 8 mo is depicted in *SI Appendix*, Fig. S14. The results suggest that for a 6-mo time interval before the first booster dose, the concentration of [PD1-PDL1] has lower values, which results in increased production of all types of memory cells (Fig. 7). Recent publications have attributed the improvement in the antibody response with delayed booster dosing to greater affinity maturation (24), but our model does not account for this mechanism.

A second booster vaccination can further increase immunity in patients on immunosuppression although the levels of memory CD4+ and CD8+ T cells and B cells are lower than those of healthy individuals after one booster vaccination (Fig. 8 for BNT-162b2a, *SI Appendix*, Figs. S12 and S13 for mRNA-1273 and AD26. COV2.S, respectively). However, model predictions suggest that the time interval of the second booster dose does not strongly affect cell immunity or the severity of viral infection. The second booster vaccination seems to be protective in the model for patients on immunosuppression regardless of when it is given in a period 3 to 6 mo following the first booster. The same conclusion was reached when we repeated simulations for all possible combinations varying the time to first and second booster from 3 to 8 mo (Fig. 9 and *SI Appendix*, Fig. S15). In Fig. 9, model predictions for the maximum values of viral load and lung microthrombi and for the minimum values of SpO2 are shown as a function of the times to the first and second booster, whereas *SI Appendix*, Fig. S15 depicts the equilibrium values after viral injection for the memory CD4+ and CD8+ T cells and B cells. Our results therefore suggest that the best interval between the first and to the second boosters is 6 mo for all vaccines.

Next, we sought to exploit the incorporation of both the humoral and the cellular immune responses in our model to explore the relative importance of these two mechanisms of vaccine-induced immunity. We repeated simulations of virus infection following a booster dose for older individuals having received the BNT-162b2a vaccine but with a zeroing out of the production of either T-cells or the B-cells. The results show that B cell deficiency results in higher viral load and microthrombi formation and lower SpO2 compared to the effect of T-cell depletion (*SI Appendix*, Fig. S16). These data are consistent with a greater importance of the humoral response to vaccine-induced immunity.

Vaccination Effectiveness against the Omicron Variants. Finally, we used the model to analyze the current SARS-CoV2 omicron variants, as well as potential future variants. Using data from neutralization experiments, we calibrated our parameter that dictates antibody-virus binding for each variant (43–46) (Fig. 10*A*). With these variant-specific parameters, we then repeated simulations for the risk of severe disease vs. time since the last injection for a first or second booster dose in immunosuppressed individuals (Fig. 10 *B* and *C* and *SI Appendix*, Fig. S17). In these simulations, we also included two hypothetical omicron-like variants we call BA.6* and BA.7* to simulate potential future
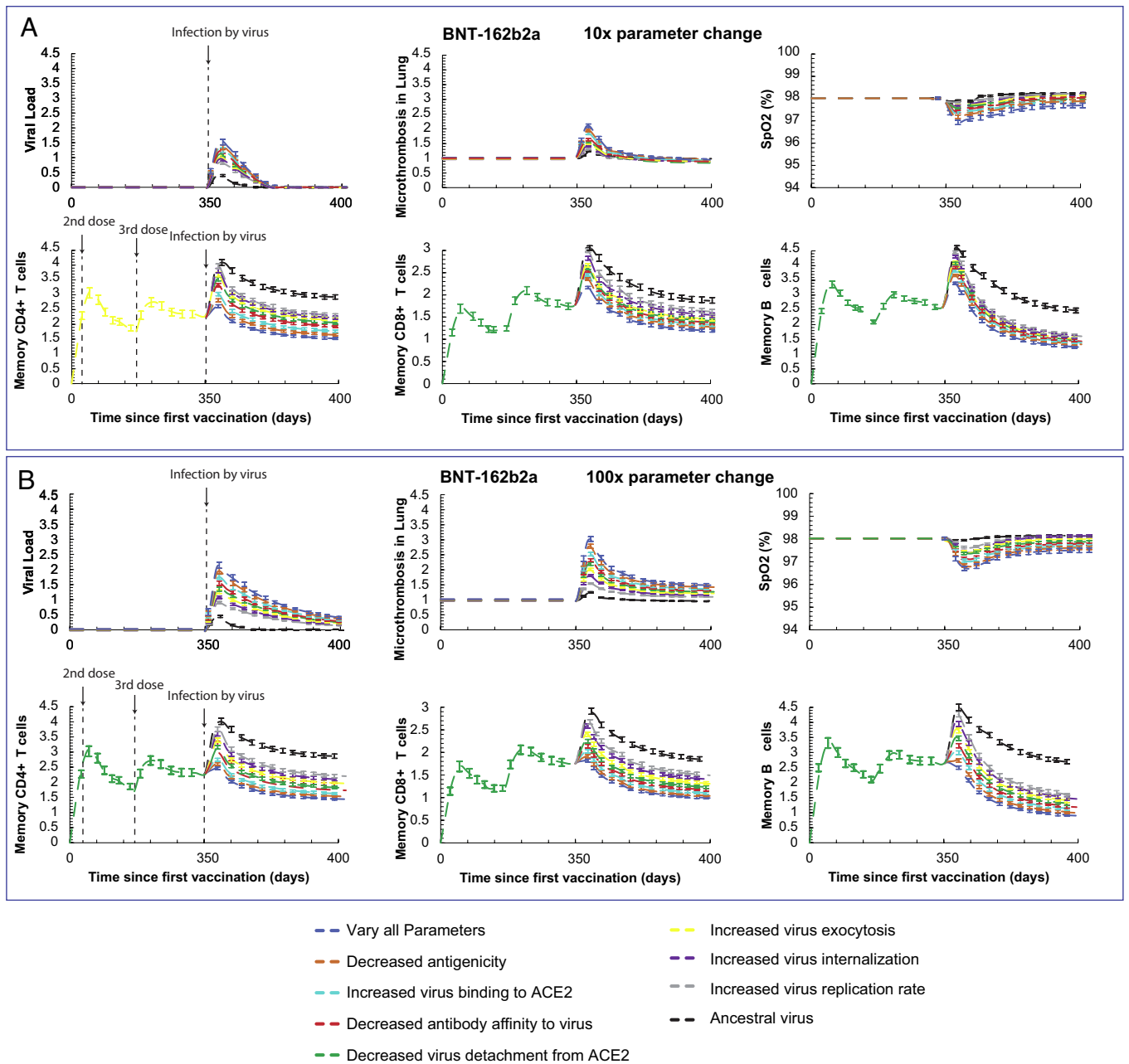
Fig. 4. Vaccine-induced protection against severe disease caused by viral variants with mild (*A*) or severe (*B*) mutations. Predictions of the viral load, coagulation/microthrombi formation in the lungs, oxygen saturation (SpO2) and the concentration of the memory CD4^{+}, CD8^{+} and B cells for breakthrough infections after BNT-162b2a vaccination and booster dose. Virus infection was assumed to take place 6 mo after the booster dose. The legend lists the parameters related to viral variants that have been varied. Normalized cell values are calculated by division with the initial value of the corresponding naïve cell type. The initial values of each naïve cell type are: immature dendritic cells 10[3] [cells], Naïve CD4^{+} T cells 10[3] [cells], Naïve CD8^{+} T cells 10[3] [cells], Naïve B cells 10[3] [cells]. The simulations were performed for mild mutations (10-fold change in parameters, *A*) and more severe mutations (100-fold changes in parameters, *B*).

mutations that might be even more immune-evasive than the extant variants. As expected, we find that variants with even lower antibody-virus affinity than BA.7* can lead to more severe infections characterized by increased viral load even with a second booster dose. However, a second booster dose results in lower viral loads, which further supports the predictions of the model for the necessity for booster doses every 6 mo for the immunosuppressed. Indeed, as a second booster provides higher protection against the omicron and its variants BA.1 to BA.4/5 but also against future, hypothetical variants, labeled BA.6*, BA.7*, that exhibit a lower degree of recognition by the antibodies of current vaccines.

In addition, we analyzed the potential benefits of vaccines generated specifically against the omicron variant. We repeated the simulations, but with a second booster dose that produced antibodies with higher binding affinity to the omicron variants (Fig. 10 *D* and *E*). For these simulations, we only increased the virus binding rate of antibodies produced by the second booster, so that we had two types of antibodies: one produced by the initial vaccinations and another induced by the second booster. We modeled virus infection 6 mo after the second booster for both immunosuppressed patients and healthy individuals and assessed the effect of modulating the degradation rate of virus by antibodies over a range from 1 to 10,000 fold. Our model predictions indicate that booster doses with the new vaccines will benefit the at-risk population more than the healthy people.
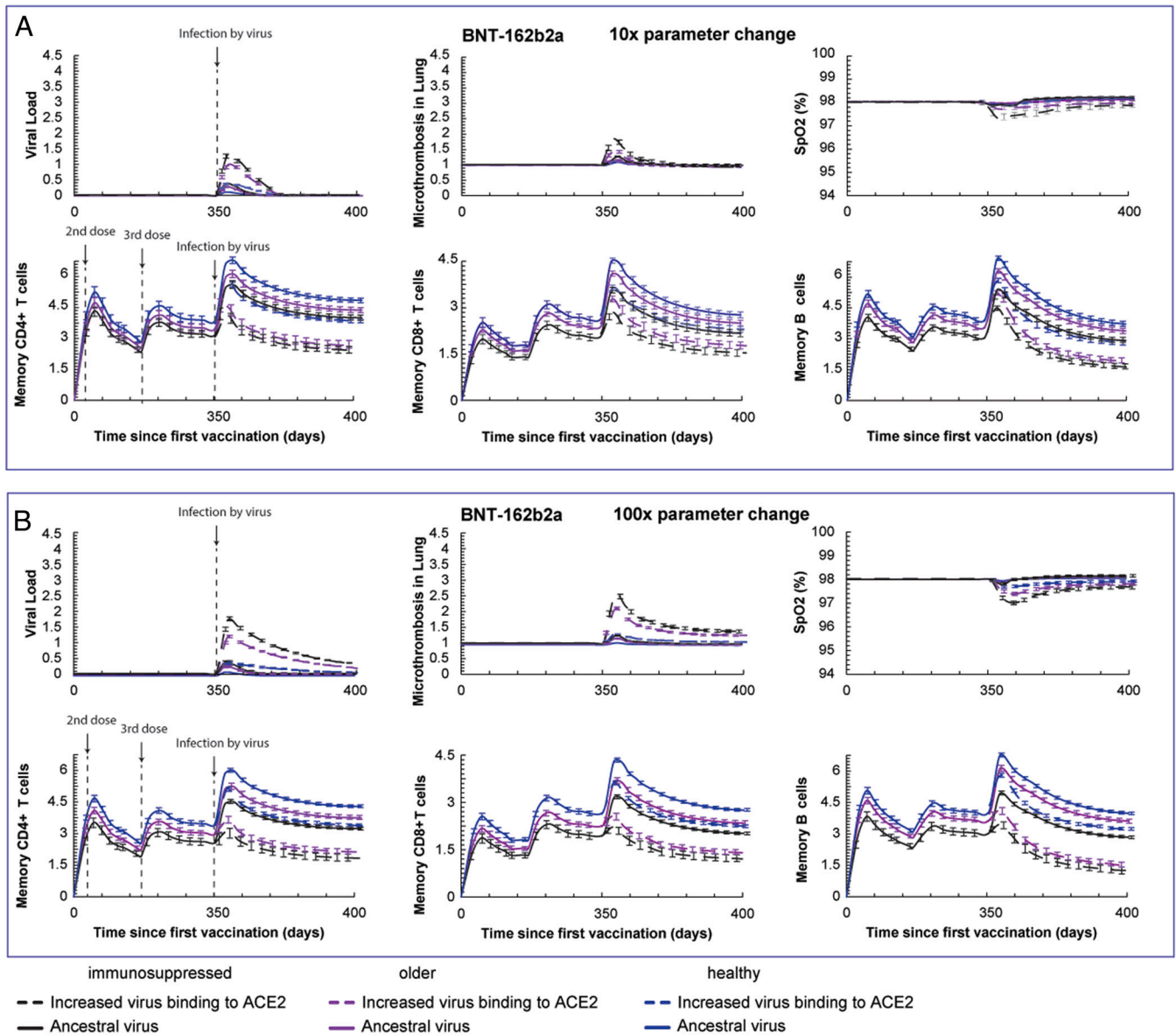
Fig. 5. Vaccine (BNT-162b2a)-induced protection against severe disease caused by viral variants with mild (*A*) or severe (*B*) mutations in ACE2 binding for healthy, older, and immunosuppressed. Predictions of the viral load, coagulation/microthrombi formation in the lungs, oxygen saturation (SpO2), and the concentration of the memory CD4$^+$, CD8$^+$, and B cells for breakthrough infections after BNT-162b2a vaccination and booster dose. Virus infection was assumed to take place 6 mo after the booster dose. Normalized cell values are calculated by division with the initial value of the corresponding naïve cell type. The initial values of each naïve cell type are: immature dendritic cells 10^3 [cells], Naïve CD4$^+$ T cells 10^3 [cells], Naïve CD8$^+$ T cells 10^3 [cells], Naïve B cells 10^3 [cells]. The simulations were performed for mild mutations (10-fold change in parameter, *A*) and more severe mutations (100-fold change in parameter, *B*).

Discussion

Vaccination is an effective measure against SARS-CoV-2 infection and the development of COVID-19, but its effectiveness may wane over time and can be limited by virus or patient-specific factors. Here, we developed a mathematical framework incorporating the known mechanisms of vaccination-induced immunity, SARS-CoV-2 infection, and COVID-19 pathophysiology to investigate the effect of booster doses on humoral and cell-mediated immunity and severity of clinical course following infection with ancestral and variant viruses. Focusing only on homologous vaccinations (i.e., no mixing of different vaccine types), we confirmed the known advantages of mRNA vaccines over vector vaccines and replicated the decreased immune response 6 mo after vaccination. A booster dose of both mRNA vaccines can induce a robust enhancement of both antibody levels and numbers of pertinent types of adaptive immune cells, which is predicted to provide sufficient protection

for more than 1 y in healthy individuals. However, our model suggests that for immunosuppressed people or patients with cancer receiving an immunosuppressive treatment (e.g., chemotherapy or B cell depletion treatment), the booster effect may wane, and perhaps should be considered on a more frequent basis.

Our analysis reinforces current CDC guidance that all individuals benefit from a booster dose after their vaccination with mRNA vaccines, and immunosuppressed and older individuals should be further considered for more frequent booster doses. For the Ad26.COV2.S vector vaccine, additional booster doses should be considered for all individuals.

Patients with cancer and/or immunosuppression are at higher risk of severe outcomes from COVID-19, and are notably at higher risk of failing to clear the virus. For this reason, it is highly important to ensure protection in this patient population. Our model simulations suggest that these groups warrant tailored approaches to vaccination, in particular, considering additional doses beyond a
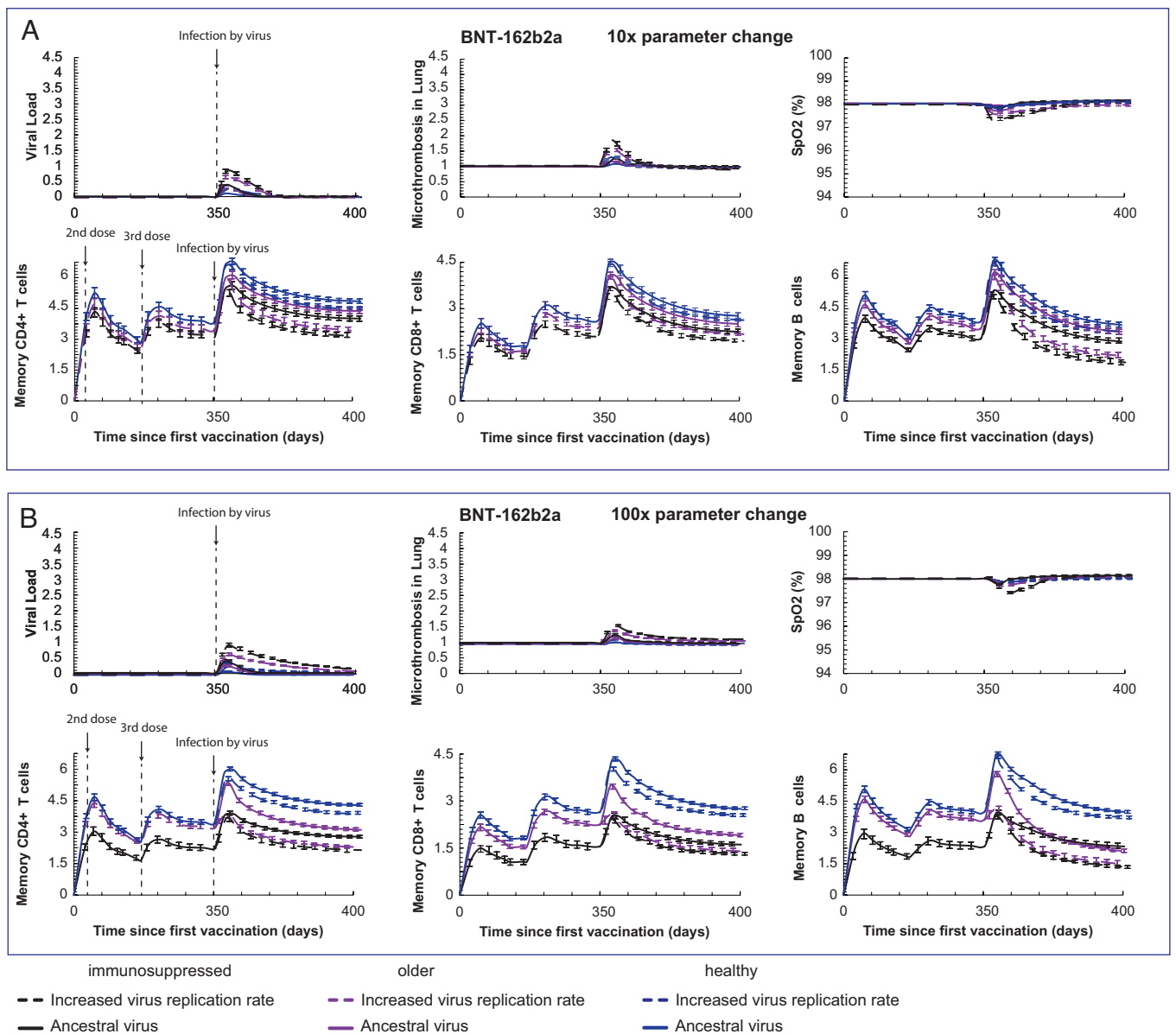
Fig. 6. Vaccine (BNT-162b2a)-induced protection against severe disease caused by viral variants with mild (*A*) or severe (*B*) mutations in virus replication ability for healthy, older, and immunosuppressed. Predictions of the viral load, coagulation/microthrombi formation in the lungs, oxygen saturation (SpO2) and the concentration of the memory CD4$^+$, CD8$^+$, and B cells for breakthrough infections after BNT-162b2a vaccination and booster dose. Virus infection was assumed to take place 6 mo after the booster dose. Normalized cell values are calculated by division with the initial value of the corresponding naïve cell type. The initial values of each naïve cell type are: immature dendritic cells 10^3 [cells], Naïve CD4$^+$ T cells 10^3 [cells], Naïve CD8$^+$ T cells 10^3 [cells], Naïve B cells 10^3 [cells]. The simulations were performed for mild mutations (10-fold change in parameter, *A*) and more severe mutations (100-fold change in parameter, *B*).

first booster dose, prioritization for next-generation vaccine approaches and consideration of additional prophylactic measures. As shown in our simulations with the severe mutation variant (Fig. 7 and *SI Appendix*, Figs. S10 and S11), the timing of the booster dose affects the induction of immunity. Therefore, it is also important to consider that different patients (with or without cancer) will need different timing of vaccination. Another interesting finding of our model is that in patients with cancer on immune checkpoint inhibition, the vaccine-mediated protection is similar to healthy individuals (*SI Appendix*, Fig. S18). Immune checkpoint inhibition and reactivation of CD8$^+$ T cell responses could lead to increased side effects, including immunopathology. Our model does not predict this effect, which complements a recent study (27) suggesting that the majority of the immunopathology in COVID-19 is cytokine mediated and thus, has limited sensitivity to checkpoint inhibition therapies.

Our model is also able to make predictions on the impact of new SARS-CoV-2 variants on COVID-19 infection. The simulations suggest that variants with enhanced target cell binding, reduced antibody binding, or reduced antigenicity/immunogenicity will present the greatest clinical challenges, even resulting in severe infections in healthy vaccinated individuals. Such variants reduce the protection afforded by the current vaccines, requiring additional booster doses or improved vaccine formulations. We anticipate that this model could be adapted to fit other variants with differing features of immune escape or viral fitness. While we focus on data available from patients infected with Omicron and its variants, the main goal of this work is to model the types of viral changes that alter vaccine response, and thus may be helpful in predicting which variants are particularly problematic from the perspective of vaccine-induced immunity.

There are a number of limitations in the analysis presented here. It depends upon a large number of parameters whose values are not
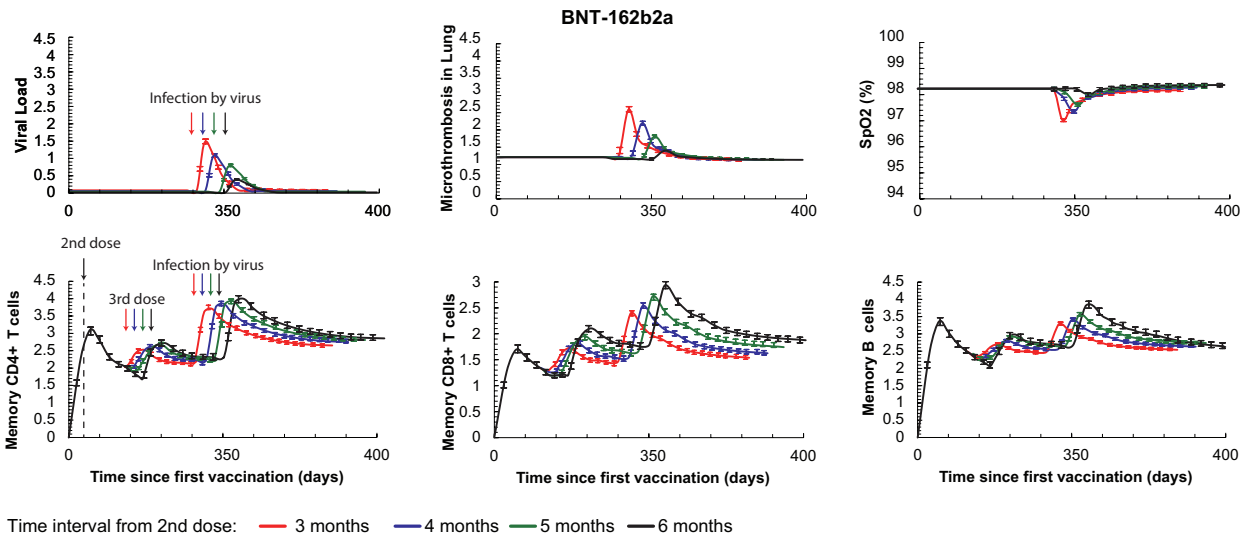
Fig. 7. Model predictions for the effect of the timing of the first booster on vaccine-induced protection. Predictions of the viral load, coagulation/microthrombi formation in the lungs, oxygen saturation (SpO2), and the concentration of the memory CD4$^+$, CD8$^+$, and B cells for breakthrough infections after BNT-162b2a vaccination for intervals between the 2nd and 3rd dose of 3 to 6 mo. Virus infection was assumed to take place 6 mo after the booster dose. Normalized cell values are calculated by division with the initial value of the corresponding naïve cell type. Error bars present the SE for all values of model parameters considered in order to account for interpatient heterogeneity. The initial values of each naïve cell type are: immature dendritic cells 10^3 [cells], Naïve CD4$^+$ T cells 10^3 [cells], Naïve CD8$^+$ T cells 10^3 [cells], Naïve B cells 10^3 [cells].

explicitly known for the SARS-CoV-2 virus. Here, and in our previous research, we have performed a robust sensitivity analysis of all major parameters of the model and have shown that model predictions might change quantitatively, but our conclusions are not affected qualitatively (28, 47). In our approach, parameters are altered according to mechanistic hypotheses on the interaction between model components and outcome, which allows for direct testing of multiple hypotheses but at the cost of increased complexity.

Our analysis is also limited in studying the effects of cancer and immunosuppressive agents. It is clear there is large variability in the effects of cancer types (e.g., hematologic cancers vs. solid tumors) on antibody production after vaccination (13). In our analysis, we did not distinguish the immunosuppressive effects of solid

tumors from hematologic malignancies. Similarly, different chemotherapy or immunotherapy strategies are likely to produce differential effects on immune cell populations and antibody response that may meaningfully affect antibody levels. It is also known that specific chemotherapies are immunostimulatory (48), whereas we have considered only those that are immunosuppressive. However, our clinical validations sets were largely pan-cancer studies without granular detail on specific therapies, and thus we developed a more general model that can be refined as more disease-specific data become available.

In conclusion, utilizing existing clinical data and mathematical modeling, we provide predictions for vaccine efficacy over time frames that greatly exceed available clinical data. Our models predict
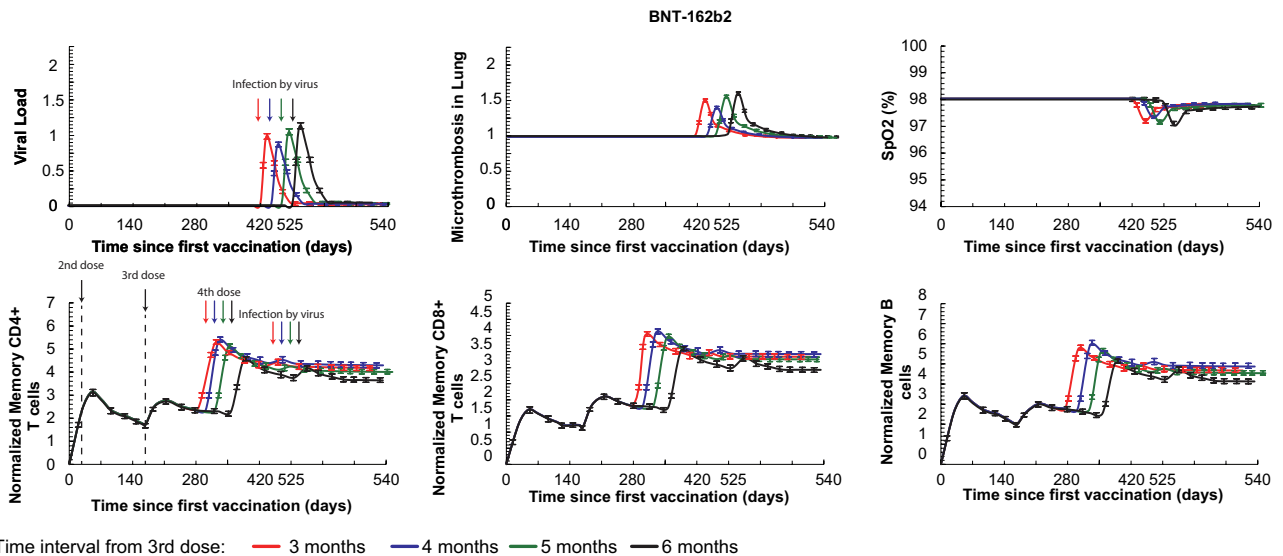
Fig. 8. Model predictions for the effect of the timing of the second booster on vaccine-induced protection. Predictions of the viral load, coagulation/microthrombi formation in the lungs, oxygen saturation (SpO2), and the concentration of the memory CD4$^+$, CD8$^+$, and B cells for breakthrough infections after BNT-162b2a vaccination for intervals between the 3rd and 4th dose of 3 to 6 mo. Virus infection was assumed to take place 6 mo after the booster dose. Normalized cell values are calculated by division with the initial value of the corresponding naïve cell type. Error bars present the SE for all values of model parameters considered in order to account for interpatient heterogeneity. The initial values of each naïve cell type are: immature dendritic cells 10^3 [cells], Naïve CD4$^+$ T cells 10^3 [cells], Naïve CD8$^+$ T cells 10^3 [cells], Naïve B cells 10^3 [cells].

Fig. 9. Diagrams of maximum viral load and microthrombosis in the lung and minimum oxygen saturation (SpO2) levels caused by viral infection as a function of the time to 1st and 2nd booster vaccinations for all type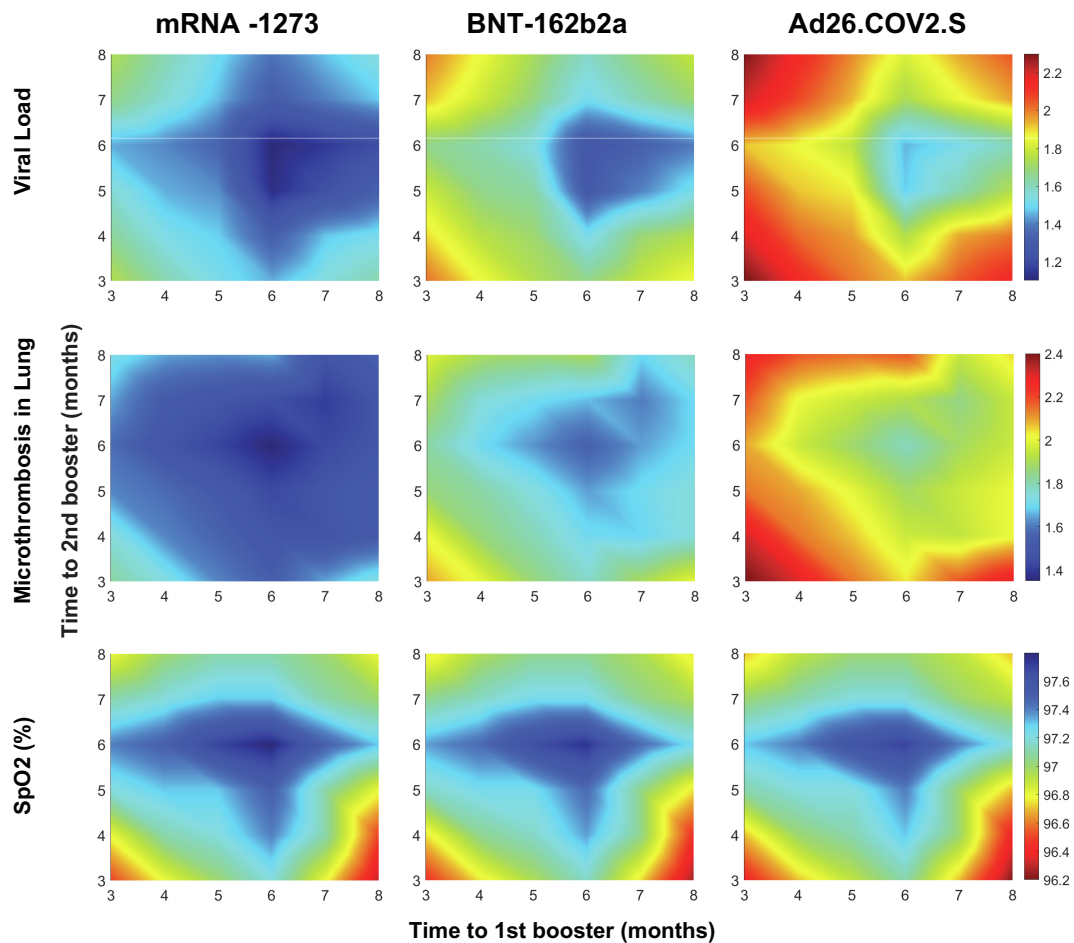s of vaccines and for immunosuppressed individuals. Virus infection was assumed to take place 6 mo following 2nd booster dose.

that variants that reduce immunogenicity, increase ACE2 binding, and decrease antibody-virus binding pose the greatest risk, but tailoring vaccine booster timing may optimize their deployment further. These results could help inform the timing of booster vaccinations in individuals of different phenotypes and comorbidities, as well as for new viral variants. As we approach an endemic phase of SARS-CoV-2, a rational approach to vaccine booster utilization may help ensure equitable access to vaccines and help prevent further outbreaks and development of new variants.

Model Description. We developed a mechanistic model of COVID-19 immunity and infection based on previous research (28) and used this to explore how variations in viral, host, and vaccine characteristics may affect COVID-19 outcomes. The model incorporates the infection of lung epithelium by SARS-CoV-2, the response of innate and adaptive immune cells to infection, the production of pro-and anti-inflammatory cytokines, the activation of the coagulation cascade, as well as the proliferation of cancer cells. The model further accounts for the interactions between the virus, the immune cells and the tumor cells, as well as for vaccination-induced immunity (Fig. 1). The basic components of the model are:
Virus infection. SARS-CoV-2 enters the cell by docking to ACE2, a key component of the Renin-angiotensin system. ACE2 can be membrane-bound or soluble, and it regulates inflammation by converting Ang II to Ang 1-7 and Ang I to Ang 1-9 (28). Intracellular virus initiates inflammatory pathways through toll-like receptors and NFκB, which produces interferons and other inflammatory cytokines. The viral antigens, along with

inflammatory cytokines, facilitate activation of naïve T and B cells, creating virus-specific T and B effector cells. T and B cell activation is controlled by viral antigen strength and the status of immune checkpoint inhibition (specifically PD-L1 / PD-1). In the presence of inflammatory cytokines and virus, neutrophils can produce neutrophil extracellular traps (NETs).
Vaccination-induced immunity. The model considers separately the mechanisms of mRNA and vector vaccines. The vaccines, as particles, either lipid nanoparticles in the case of mRNA vaccines or viral-vector in the case of vector vaccines, enter host cells and either induce DNA transcription to mRNA (vector vaccine) and then translation into viral antigen or result directly in translation of viral antigens (mRNA vaccine). Subsequently, vaccine-induced peptides exit the cells and interact with dendritic cells to produce APCs. These subsequently activate T cells and B cells to create CD4+ and CD8+ effector and memory T cells as well as short-lived and long-lived plasma (antibody-secreting) B cells.
Coagulation cascade. The virus can infect endothelial cells and disseminate via the blood stream, with the possibility of systemic infection and thrombosis. Infection of endothelial cells, combined with high levels of inflammatory cytokines in the plasma, can result in thrombosis. Damage to virally infected endothelial cells and the production of NETs can exacerbate the thrombosis, and microthrombi can enter the blood stream to accumulate in other organs, including the brain, heart, and lung. We use a simplified model of the coagulation pathways, assuming that formation of microthrombi is proportional to the number of infected endothelial cells, the presence of neutrophil NETs, and the level
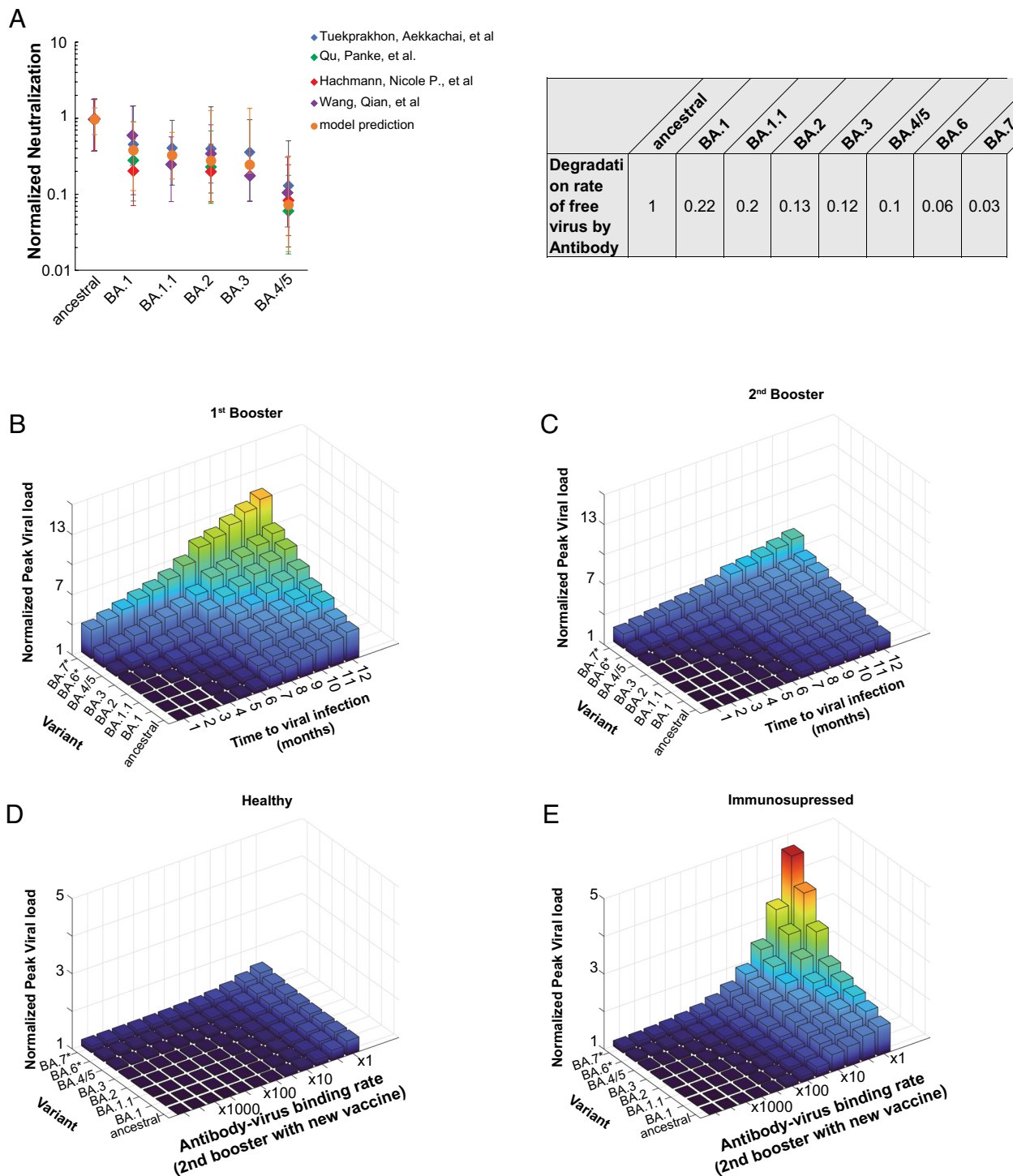
Fig. 10. (*A*) Model comparison with clinical data of neutralization for the ancestral and the omicron variants. Clinical data of neutralization essays were employed to fit the model and determine the degradation rate of free virus by antibodies produced by vaccination. The experiments were simulated having the virus to be killed only by antibodies produced after a first booster dose. In the plot, the kite scatter symbols correspond to clinical data (43–46) and the circle to model predictions. Error bars present the SE of antibody concentration for the range of values of model parameters considered (*SI Appendix*, Table S1). The table presents the values of the model parameter for the degradation rate of the free virus by the antibodies found by the fitting of the model to the experimental data. The values are normalized to the baseline value of the ancestral. (*B* and *C*) After we defined the degradation rate by antibodies for each variant, we simulated viral infection following a first or a second booster dose as a function of time to last injection for immunosuppressed. Diagrams depict the normalized peak viral load caused by viral infection. The results further support the necessity for booster doses every 6 mo for the immunosuppressed. (*D* and *E*) Diagrams of normalized peak viral load caused by viral infection as a function of the degradation rate of free virus by antibody after a second booster dose with vaccines with increased killing potential against the omicron variants. In the simulations, the previous injections involved the BNT-162b2a vaccine. Simulations were performed for healthy and immunosuppressed individuals. The second booster dose was administered 6 mo after the first booster and virus infection was set 6 mo later.

of inflammatory cytokines. Transport of oxygen from the alveolar space to the blood vessels in the lung is calculated using a modified diffusion model, which accounts for damage-induced thickening of the alveolar membrane.

PK/PD model. The PK/PD model has been formulated to incorporate major organs: lung, heart, liver, brain, spleen, gastrointestinal, upper body, lower body, torso, cardiac vessels. The tumor is also incorporated in the PK/PD model as a separate

organ. The PK/PD model allows for systemic transport of viral particles, antibodies, cytokines, and microthrombi among these compartments (*SI Appendix*, Fig. S19).

Tumor progression. Cancer cell proliferation depends on the oxygen levels in the tissue, and their death rate depends on the interaction of cancer cells with immune cells (effector CD8+ T cells, natural killer cells, type 1 macrophages and neutrophils) as well as on the effect of cancer therapy (49, 50). We assume that cancer cells are not infected by the virus.

A detailed description of model equations, the description and values of model parameters, and the solution strategy are provided in *SI Appendix*.

Code Availability. The COMSOL code is available at Zenodo (https://doi.org/10.5281/zenodo.7475990).

Data, Materials, and Software Availability. All data supporting the findings of this study are available in the article and the *SI Appendix*.

Author affiliations: [a]Edwin L Steele Laboratories, Department of Radiation Oncology, Massachusetts General Hospital and Harvard Medical School, Boston, MA, 02114; [b]Cancer Biophysics Laboratory, Department of Mechanical and Manufacturing Engineering, University of Cyprus, Nicosia, Cyprus, 2238; [c]Department of Pulmonary and Critical Care Medicine, Massachusetts General Hospital and Harvard Medical School, Boston, MA, 02114; [d]Massachusetts General Hospital Cancer Center, Division of Hematology/Oncology, Department of Medicine, Massachusetts General Hospital, Boston, MA, 02114; [e]Dana-Farber Cancer Institute, Boston, MA, 02215; [f]Center for the AIDS Programme of Research in South Africa, Durban, South Africa, 4001; [g]Department of Mechanical Engineering, Sharif University of Technology, Tehran, Iran, 5501; and [h]Department of Radiation Oncology, Massachusetts General Hospital and Harvard Medical School, Boston, MA, 02114

1. B. Choi *et al.*, Persistence and evolution of SARS-CoV-2 in an immunocompromised host. *N Engl. J. Med.* **383**, 2291–2293 (2021).
2. F. Karim *et al.*, Persistent SARS-CoV-2 infection and intra-host evolution in association with advanced HIV infection. MedRxiv (2021) https://doi.org/10.1101/2021.06.03.21258228 June 04, 2021.
3. L. J. Abu-Raddad *et al.*, Association of prior SARS-CoV-2 infection with risk of breakthrough infection following mRNA vaccination in Qatar. *JAMA* **326**, 1930–1939 (2021).
4. P. J. Embi *et al.*, Effectiveness of 2-dose vaccination with mRNA COVID-19 vaccines against COVID-19-associated hospitalizations among immunocompromised adults– Nine states, January–September 2021. *MMWR Morb Mortal Wkly Rep.* **70**, 1553–1559 (2021).
5. C. H. Bozio *et al.*, Laboratory-confirmed COVID-19 among adults hospitalized with COVID-19-like illness with infection-induced or mRNA vaccine-induced SARS-CoV-2 immunity–Nine states, January–September 2021. *MMWR Morb Mortal Wkly Rep.* **70**, 1539–1544 (2021).
6. O. Van Oekelen *et al.*, Highly variable SARS-CoV-2 spike antibody responses to two doses of COVID-19 RNA vaccination in patients with multiple myeloma. *Cancer Cell* **39**, 1028–1030 (2021).
7. Y. Goldberg *et al.*, Waning Immunity after the BNT162b2 Vaccine in Israel. *N Engl. J. Med.* **385**, e85 (2021).
8. A. Thakkar *et al.*, Seroconversion rates following COVID-19 vaccination among patients with cancer. *Cancer Cell* **39**, 1081–1090.e1082 (2021).
9. V. G. Hall *et al.*, Randomized trial of a third dose of mRNA-1273 vaccine in transplant recipients. *N Engl. J. Med.* **385**, 1244–1246 (2021).
10. A. Massarweh *et al.*, Evaluation of seropositivity following BNT162b2 messenger RNA vaccination for SARS-CoV-2 in patients undergoing treatment for cancer. *JAMA Oncol.* **7**, 1133–1140 (2021).
11. A. Addeo *et al.*, Immunogenicity of SARS-CoV-2 messenger RNA vaccines in patients with cancer. *Cancer Cell* **39**, 1091–1098 e1092 (2021).
12. V. Naranbhai, Comparative immunogenicity and effectiveness of mRNA-1273, BNT162b2 and Ad26.COV2.S COVID-19 vaccines. medRxiv (2021) https://doi.org/10.1101/2021.07.18.21260732 October 13, 2021.
13. V. Naranbhai *et al.*, Immunogenicity and reactogenicity of SARS-CoV-2 vaccines in patients with cancer: The CANVAX cohort study. *J. Clin. Oncol.* **40**, 12–23 (2022).
14. V. Naranbhai *et al.*, Neutralization breadth of SARS-CoV-2 viral variants following primary series and booster SARS-CoV-2 vaccines in patients with cancer. *Cancer Cell* **40**, 103–108.e102 (2022).
15. R. E. Chen *et al.*, Reduced antibody activity against SARS-CoV-2 B.1.617.2 delta virus in serum of mRNA-vaccinated individuals receiving tumor necrosis factor-alpha inhibitors. *Med (N Y)* **2**, 1327–1341.e4 (2021).
16. P. Shenoy *et al.*, Hybrid immunity versus vaccine-induced immunity against SARS-CoV-2 in patients with autoimmune rheumatic diseases. *Lancet Rheumatol.* **4**, e80–e82 (2022).
17. Y. Rottenberg *et al.*, Assessment of response to a third dose of the SARS-CoV-2 BNT162b2 mRNA vaccine in patients with solid tumors undergoing active treatment. *JAMA Oncol.* **8**, 300–301 (2022).
18. N. Kamar *et al.*, Assessment of 4 doses of SARS-CoV-2 messenger RNA-based vaccine in recipients of a solid organ transplant. *JAMA Netw. Open* **4**, e2136030 (2021).
19. J. D. Challenger *et al.*, Modelling upper respiratory viral load dynamics of SARS-CoV-2. *BMC Med.* **20**, 25 (2022).
20. P. Padmanabhan, R. Desikan, N. M. Dixit, Modeling how antibody responses may determine the efficacy of COVID-19 vaccines. *Nat. Comput. Sci.* **2**, 123–131 (2022).
21. V. I. Zarnitsyna, J. F. Gianlupi, A. Hagar, T. J. Sego, J. A. Glazier, Advancing therapies for viral infections using mechanistic computational models of the dynamic interplay between the virus and host immune response. *Curr. Opin. Virol.* **50**, 103–109 (2021).
22. L. Zhang, R. Li, G. Song, G. D. Scholes, Z. S. She, Impairment of T cells' antiviral and anti-inflammation immunities may be critical to death from COVID-19. *R. Soc. Open Sci.* **8**, 211606 (2021).
23. R. Desikan, P. Padmanabhan, A. M. Kierzek, P. H. van der Graaf, Mechanistic models of COVID-19: Insights into disease progression, vaccines, and therapeutics. *Int. J. Antimicrob. Agents* **60**, 106606 (2022).
24. A. K. Garg, S. Mittal, P. Padmanabhan, R. Desikan, N. M. Dixit, Increased B cell selection stringency in germinal centers can explain improved COVID-19 vaccine efficacies with low dose prime or delayed boost. *Front immunol.* **12**, 4917089 (2021).
25. N. Néant *et al.*, Modeling SARS-CoV-2 viral kinetics and association with mortality in hospitalized patients from the French COVID cohort. *Proc. Natl. Acad. Sci. U.S.A.* **118**, e2017962118 (2021).
26. M. Prague, Q. Clairon, J. Guedj, R. Thiebaut, Modeling brings additional insights into the kinetics of SARS-CoV-2 neutralizing antibody. medRxiv (2021) https://doi.org/10.1101/2021.10.13.21264693 October 20, 2021.
27. B. Chatterjee, H. Singh Sandhu, N. M. Dixit, Modeling recapitulates the heterogeneous outcomes of SARS-CoV-2 infection and quantifies the differences in the innate immune and CD8 T-cell responses between patients experiencing mild and severe symptoms. *PLoS Pathogens* **18**, e1010630 (2022).
28. C. Voutouri *et al.*, In silico dynamics of COVID-19 phenotypes for optimizing clinical management. *Proc. Natl. Acad. Sci. U.S.A.* **118**, e2021642118. (2021).
29. L. S. Mayorga, M. Verma, R. Hontecillas, S. Hoops, J. Bassaganya-Riera, Agents and networks to model the dynamic interactions of intracellular transport. *Cell Logist* **7**, e1392401 (2017).
30. A. Arazi, W. F. Pendergraft III, R. M. Ribeiro, A. S. Perelson, N. Hacohen, Human systems immunology: Hypothesis-based modeling and unbiased data-driven approaches. *Semin. Immunol.* **25**, 193–200 (2013).
31. Y. Vodovotz *et al.*, Solving immunology? *Trends Immunol.* **38**, 116–127 (2017).
32. D. S. Khoury *et al.*, Neutralizing antibody levels are highly predictive of immune protection from symptomatic SARS-CoV-2 infection. *Nat. Med.* **27**, 1205–1211 (2021).
33. L. C. Shapiro *et al.*, Efficacy of booster doses in augmenting waning immune responses to COVID-19 vaccine in patients with cancer. *Cancer Cell* **40**, 3–5 (2022).
34. S. Ehmsen *et al.*, Antibody responses following third mRNA COVID-19 vaccination in patients with cancer and potential timing of a fourth vaccination. *Cancer Cell* **40**, 338–339 (2022).
35. Z. Zhang *et al.*, Humoral and cellular immune memory to four COVID-19 vaccines. *Cell* **185**, 2434–2451.e2417 (2022).
36. A. R. Falsey *et al.*, SARS-CoV-2 neutralization with BNT162b2 vaccine dose 3. *N Engl. J. Med.* **385**, 1627–1629 (2021).
37. L. Yue *et al.*, A third booster dose may be necessary to mitigate neutralizing antibody fading after inoculation with two doses of an inactivated SARS-CoV-2 vaccine. *J. Med. Virol.* **94**, 35–38 (2022).
38. R. Lassauniere *et al.*, Neutralizing antibodies against the SARS-CoV-2 omicron variant (BA.1) 1 to 18 weeks after the second and third doses of the BNT162b2 mRNA vaccine. *JAMA Netw. Open* **5**, e2212073 (2022).
39. A. P. Munro *et al.*, Safety, immunogenicity, and reactogenicity of BNT162b2 and mRNA-1273 COVID-19 vaccines given as fourth-dose boosters following two doses of ChAdOx1 nCoV-19 or BNT162b2 and a third dose of BNT162b2 (COV-BOOST): A multicentre, blinded, phase 2, randomised trial. *Lancet Infect. Dis.* **22**, 1131–1141 (2022).
40. I. W. Windsor *et al.*, Antibodies induced by ancestral SARS-CoV-2 strain that cross-neutralize variants from Alpha to Omicron BA. 1. *Sci. Immunol.* **7**, eabo3425 (2022).
41. R. Pajon *et al.*, SARS-CoV-2 omicron variant neutralization after mRNA-1273 booster vaccination. *N. Engl. J. Med.* **386**, 1088–1091 (2022).
42. N. P. Hachmann *et al.*, Neutralization escape by SARS-CoV-2 omicron subvariants BA.2.12.1, BA.4, and BA.5. *N. Engl. J. Med.* **387**, 86–88 (2022).
43. Q. Wang, Antibody evasion by SARS-CoV-2 omicron subvariants BA. 2.12. 1, BA. 4 and BA. 5. *Nature* **608**, 603–608 (2022).
44. N. P. Hachmann, Neutralization escape by SARS-CoV-2 omicron subvariants BA. 2.12. 1, BA. 4, and BA. 5. *New Engl. J. Med.* **387**, 86–88 (2022).
45. P. Qu *et al.*, Neutralization of the SARS-CoV-2 omicron BA. 4/5 and BA. 2.12. 1 subvariants. *N. England J. Med.* **386**, 2526–2528 (2022).
46. A. Tuekprakhon, Antibody escape of SARS-CoV-2 omicron BA. 4 and BA. 5 from vaccine and BA. 1 serum. *Cell* **185**, 2422–2433. e2413 (2022).
47. S. Subudhi *et al.*, Strategies to minimize heterogeneity and optimize clinical trials in acute respiratory distress syndrome (ARDS): Insights from mathematical modelling. *EBioMedicine* **75**, 103809 (2022).
48. L. Galluzzi, J. Humeau, A. Buque, L. Zitvogel, G. Kroemer, Immunostimulation with chemotherapy in the era of immune checkpoint inhibitors. *Nat. Rev. Clin. Oncol.* **17**, 725–741 (2020).
49. C. Voutouri *et al.*, Experimental and computational analyses reveal dynamics of tumor vessel cooption and optimal treatment strategies. *Proc. Natl. Acad. Sci. U.S.A.* **116**, 2662–2671 (2019).
50. F. Mpekris *et al.*, Combining microenvironment normalization strategies to improve cancer immunotherapy. *Proc. Natl. Acad. Sci. U.S.A.* **117**, 3728–3737 (2020).